# Supplementary Information

**Design of yolk-shell ternary metal sulfide with tunable structure for high-performance electromagnetic wave absorption**

Zhaobo Liu, [a] Yan Zhao *[a] and Zhiwei Liu *[a]

[a] School of Materials Science and Engineering, Beihang University, Beijing, 100191, China

* Corresponding author E-mail addresses: jennyzhaoyan@buaa.edu.cn (Y. Zhao),

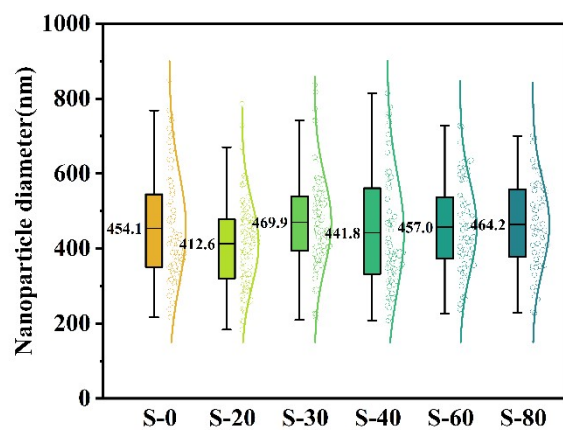* Corresponding author E-mail addresses: lzwbuaa@163.com (Z. Liu).

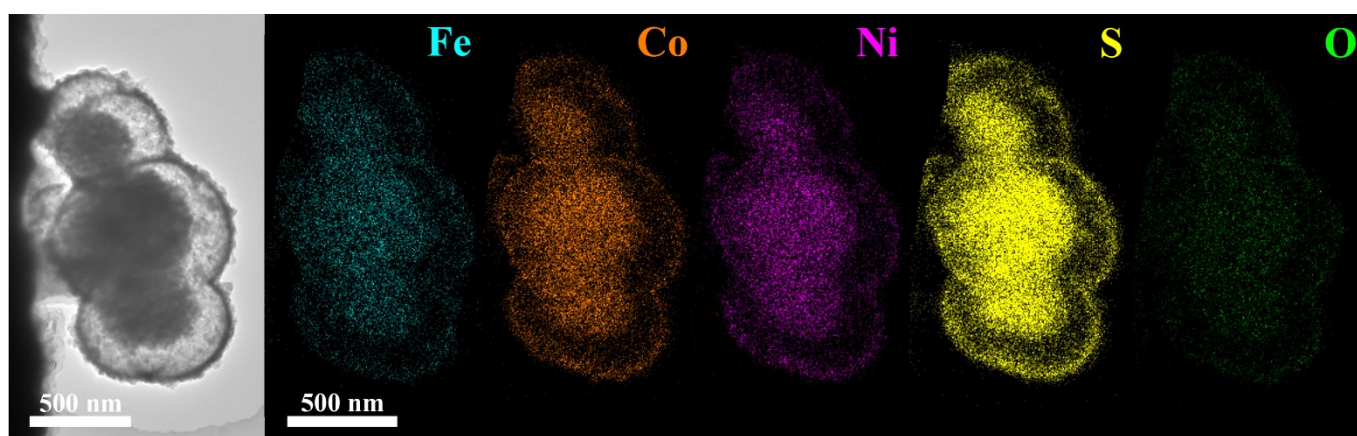**Figure S1.** Particle size distribution and average diameter of different samples



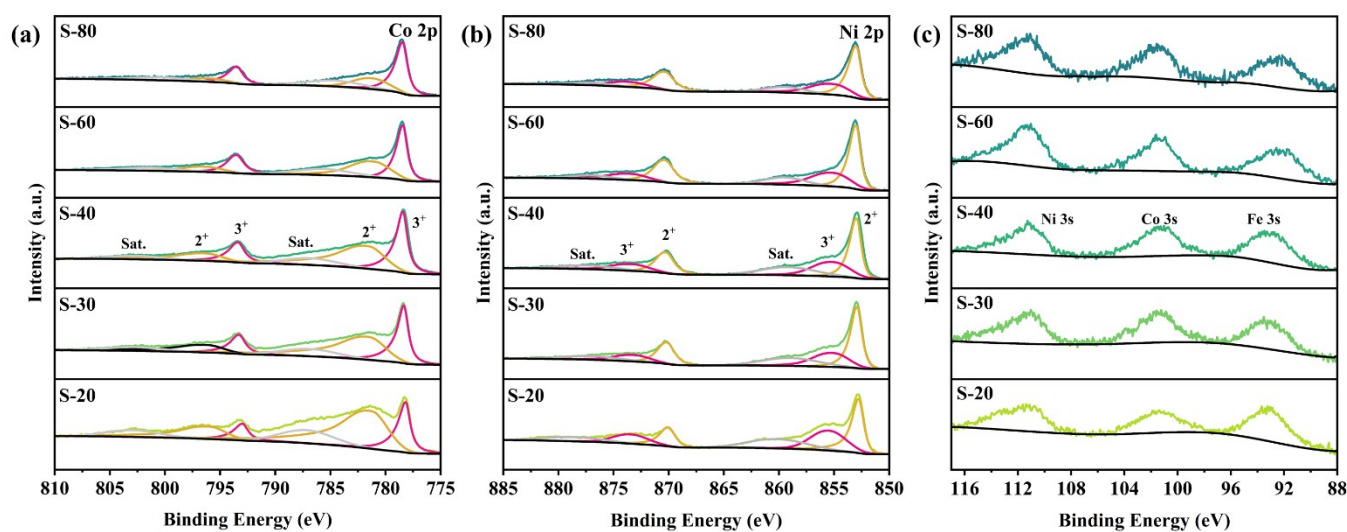**Figure S2.** Elemental mapping images of energy dispersive X-ray spectroscopy (EDS) for S-40.



**Figure S3.** Deconvoluted XPS spectra of (a) Co 2p, (b) Ni 2p, (c) Fe 3s, Co 3s and Ni 3s.
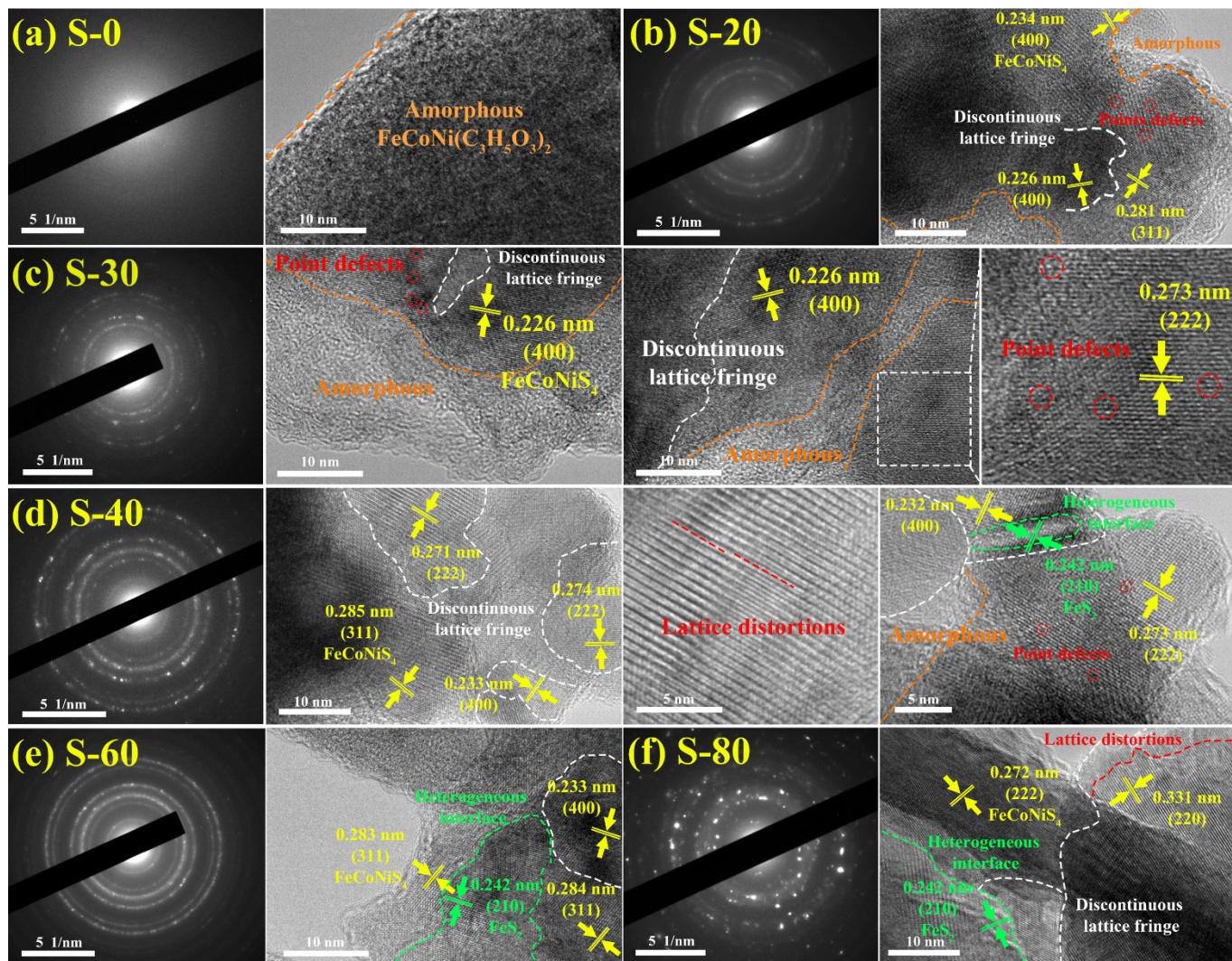
**Figure S4.** Selected area electron diffraction (SAED) patterns and high-resolution transmission electron microscopy (HR-TEM) images for (a) S-0, (b) S-20, (c) S-30, (d) S-40, (e) S-60 and (f) S-80.
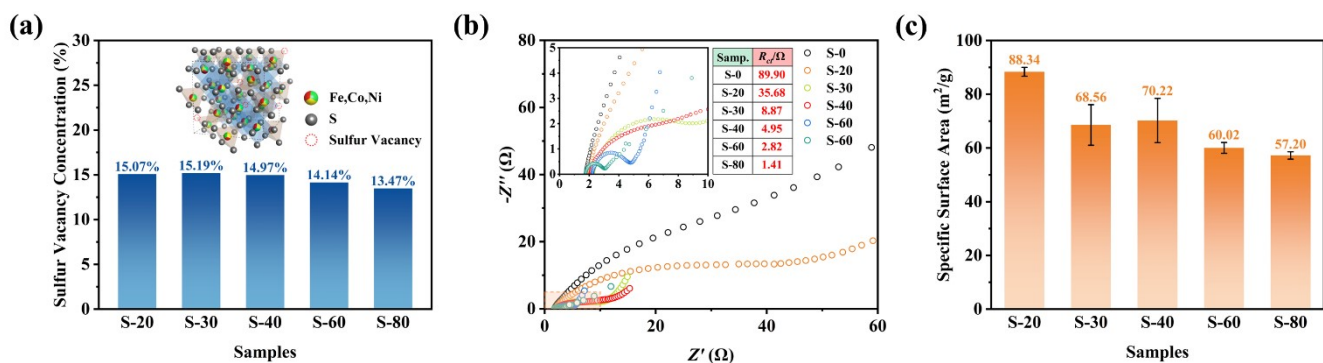


**Figure S5.** (a) Histogram of the calculated sulfur vacancy concentration; (b) Nyquist plots from the electronic impedance spectra (EIS) test; (c) Brunauer-Emmett-Teller (BET) analysis results obtained by $N_2$ adsorption-desorption measurement at 77K.
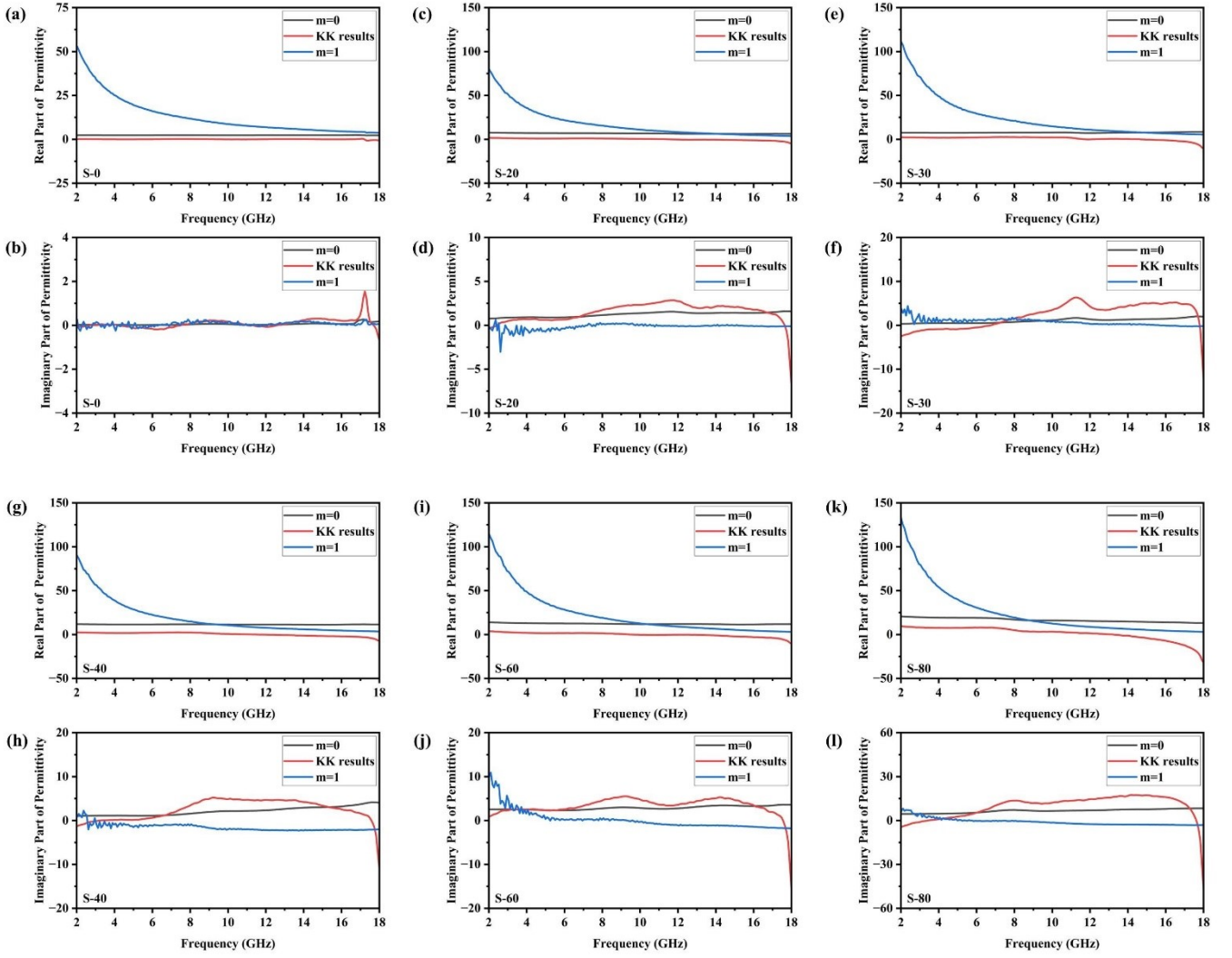
**Figure S6.** The real and imaginary parts of the permittivity of different *m* values and Kramers-Kronig (KK) analysis results for (a,b) S-0, (c,d) S-20, (e,f) S-30, (g,h) S-40 (i,j) S-60 and (k,l) S-80.

In the process of calculating permittivity based on scattering parameters, different *m* values were selected for calculation and Kramers-Kronig (KK) analysis was carried out, the results were shown in **Figure S6**. It can be obviously found that the measure results with *m*=0 agree best with the KK analysis results, which verified the validity of test results. Then we conduct the subsequent absorption performance analysis according to the dielectric parameters with *m*=0.

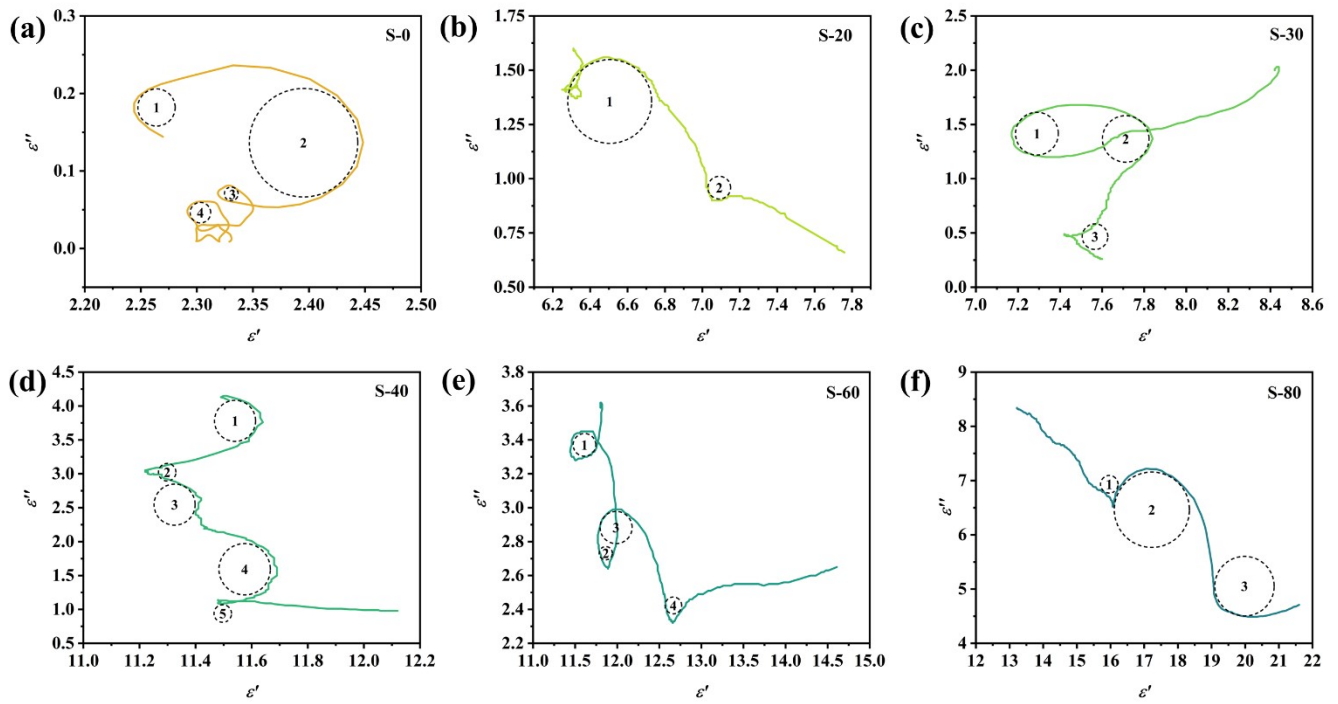**Figure S7.** Cole-Cole semicircles of (a)S-0, (b) S-20, (c) S-30, (d) S-40 (e) S-60 and (f) S-80.

**Table S1.** Comparison of standard X-ray diffraction patterns of different spinel metal sulfides

| crystallographic planes | This work $2\theta/°$ | Ni$_3$S$_4$ (PDF#01-076-1813) $2\theta/°$ | Co$_3$S$_4$ (PDF#01-072-8728) $2\theta/°$ | CoNi$_2$S$_4$ (PDF#01-073-1297) $2\theta/°$ | NiCo$_2$S$_4$ (PDF#01-073-1704) $2\theta/°$ | FeNi$_2$S$_4$ (PDF#01-073-8669) $2\theta/°$ |
|---|---|---|---|---|---|---|
| (220) | 26.8 | 26.639 | 26.786 | 26.734 | 26.841 | 26.619 |
| (311) | 31.6 | 31.346 | 31.520 | 31.459 | 31.585 | 31.322 |
| (400) | 38.3 | 38.029 | 38.243 | 38.168 | 38.323 | 38.000 |
| (422) | 47.4 | 47.036 | 47.306 | 47.210 | 47.407 | 46.999 |
| (511) | 50.4 | 50.079 | 50.369 | 50.266 | 50.477 | 50.039 |
| (440) | 55.3 | 54.873 | 55.196 | 55.081 | 55.316 | 54.829 |

**Table S2.** Comparison of Raman vibration modes in this work with references

| Ref. | A$_g$/cm$^{-1}$ | E$_g$/cm$^{-1}$ | T$_{2g,1}$/cm$^{-1}$ | T$_{2g,2}$/cm$^{-1}$ |
|---|---|---|---|---|
| This work | 376-383 | 249 | 346 | 300 |
| 1 (CoNi$_2$S$_4$) | 386 | 230 | 351 | 299 |
| 2 (FeS$_2$) | 372 | 337 | - | - |

**Table S3.** Peak areas (CPS.eV) and atomic% of Fe 3s (92.8 eV), Co 3s (101.1 eV) and Ni 3s (111.4eV) in XPS spectra of different samples

| Samples | Fe 3s (CPS.eV) | Co 3s (CPS.eV) | Ni 3s (CPS.eV) | Fe 3s ratio (%) | Co 3s ratio (%) | Ni 3s ratio (%) |
|---|---|---|---|---|---|---|
| Sensitivity factors | 0.548 | 0.606 | 0.671 | | | |
| S-20 | 8498.88 | 7623.10 | 9625.94 | 36.55 | 29.64 | 33.81 |
| S-30 | 9187.05 | 9805.61 | 11059.36 | 33.92 | 32.74 | 33.35 |
| S-40 | 9211.39 | 9559.52 | 10473.28 | 34.88 | 32.73 | 32.39 |
| S-60 | 8881.00 | 9494.73 | 11636.28 | 32.93 | 31.84 | 35.24 |
| S-80 | 6204.80 | 7005.11 | 8101.82 | 32.39 | 33.07 | 34.54 |

**Table S4.** Peak areas (CPS.eV) of S 2p, O 1s O-M (530.1 eV) in XPS spectra of different samples

| Samples | S 2p (CPS.eV) | O 1s O-M (CPS.eV) | S 2p after correction (CPS.eV) | O1s O-M after correction (CPS.eV) | FeCoNiS$_4$ ratio (%) | FeCoNi (C$_3$H$_5$O$_3$)$_2$ ratio (%) |
|---|---|---|---|---|---|---|
| Sensitivity factors | 1.881 | 2.881 | | | | |
| S-20 | 68806.70 | 100401.54 | 36579.85 | 34849.55 | 61.16 | 38.84 |
| S-30 | 115706.32 | 75597.17 | 61513.20 | 26239.91 | 77.86 | 22.14 |
| S-40 | 130895.62 | 67279.39 | 69588.31 | 23352.79 | 81.72 | 18.28 |
| S-60 | 179418.38 | 13701.87 | 95384.57 | 4755.94 | 96.78 | 3.22 |
| S-80 | 143573.18 | 3361.79 | 76328.11 | 1166.88 | 98.99 | 1.01 |

**Table S5.** Binding energies (eV) of S 2p and the calculated sulfur vacancy concentration for FeCoNiS$_x$G$_y$

| | Samples | | S-20 | S-30 | S-40 | S-60 | S-80 |
|---|---|---|---|---|---|---|---|
| | S$^{2-}$ 2p$_{3/2}$ | 161.5 (eV) | 20304.4 | 34410.05 | 38360.23 | 49667.34 | 37859.55 |
| | S$_2^{2-}$ 2p$_{3/2}$ | 162.5(eV) | 11205.47 | 20597.57 | 23897.33 | 40744.5 | 32371.62 |
| | S$^{2-}$ 2p$_{1/2}$ | 162.7 (eV) | 10371.71 | 17577.03 | 19594.83 | 25370.63 | 19339.08 |
| | S$_2^{2-}$ 2p$_{1/2}$ | 163.7 (eV) | 5723.88 | 10521.47 | 12207.02 | 20812.74 | 16535.78 |
| Area of S 2p | S-S 2p$_{3/2}$ | 164.3 (eV) | 5081.82 | 8936.93 | 9829.51 | 16266.93 | 13991.69 |
| (CPS.eV) | S-S 2p$_{1/2}$ | 165.5 (eV) | 2595.85 | 4565.08 | 5021.02 | 8309.33 | 7147.11 |
| | SO$_3^{2-}$ 2p$_{3/2}$ | 167.1 (eV) | 3500.93 | 5167.06 | 6137.81 | 5564.23 | 4479.48 |
| | SO$_3^{2-}$ 2p$_{1/2}$ | 168.3 (eV) | 1788.31 | 2639.39 | 3135.26 | 2842.27 | 2288.17 |
| | SO$_4^{2-}$ 2p$_{3/2}$ | 168.9 (eV) | 5450.27 | 7473.96 | 8414.43 | 6513.33 | 6328.19 |
| | SO$_4^{2-}$ 2p$_{1/2}$ | 170.1 (eV) | 2784.06 | 3817.78 | 4298.18 | 3327.08 | 3232.51 |
| | S$^{2-}$ 2p$_{1/2}$/S$_{total}$ (%) | | 15.07 | 15.19 | 14.97 | 14.14 | 13.47 |

# Supplementary References

1  D. Larcher, G. Sudant, R. Patrice and J. M. Tarascon, *Chem. Mat.*, 2003, **15**, 3543-3551.
2  X. Liu, M. Gong, S. Deng, T. Zhao, J. Zhang and D. Wang, *J. Mater. Chem. A.* 2020, **8**, 113-1149.